Hindawi
International Journal of Optics
Volume 2022, Article ID 2710506, 6 pages
https://doi.org/10.1155/2022/2710506

Research Article

A Simplified Method of Microscopic Polarizability Tensor Differential of Hyper-Raman Spectroscopy Based on the Bond Additivity Model

Yuan Wang[1] **and Liping Huang**[2]

[1]*Institute of Technology, University of Sanya, Sanya 572022, China*
[2]*Sanya No. 1 Middle School, Sanya 572022, China*

Correspondence should be addressed to Yuan Wang; wangyuan0155@163.com

Received 12 October 2021; Revised 7 February 2022; Accepted 15 February 2022; Published 10 March 2022

Academic Editor: Wonho Jhe

Coherent anti-Stokes Raman spectroscopy (CARS) and Ccherent anti-Stokes hyper-Raman spectroscopy (CAHRS), as other high-order nonlinear spectroscopy techniques, are widely exploited in many research fields, such as dynamic processes, gene expression spectrum screening, high-resolution spectroscopy, and nonlinear high-resolution imaging. However, it is difficult to make a quantitative analysis of the spectral signals that involve a large number of high-order micropolarizability tensors. It is reported that the CARS and CAHRS microscopic hyperpolarizability tensor elements can be decomposed into the product of the differentiation of Raman microscopic polarizability tensor $\alpha'_{i'j'}$ and hyper-Raman microscopic polarizability tensor $\beta'_{i'j'k'}$ so that the high-order spectra can be simplified to the analysis of low-order spectra. In this paper, we use the bond additivity model (BAM) combined with experimental corrections to address the carbon dioxide (CO_2) molecule and present the simplified scheme for differentiation of hyper-Raman microscopic polarizability tensor elements $\beta'_{i'j'k'}$. Taking advantage of this approach, combined with the experimental correction, the differentiation of Hyper-Raman microscopic polarizability tensor elements $\beta'_{i'j'k'}$ of the CO_2 is obtained and the expressions of $\beta'_{i'j'k'}$ for antisymmetric vibrations of CO_2 are deduced. Finally, substituting the differentiation of Raman microscopic polarizability tensor elements $\alpha'_{i'j'}$ reported in the literature into the ratio above can obtain the proportional relationship between the microscopic polarizability tensor elements of CARS and CAHRS of the CO_2. This method can provide the basis for the quantitative analysis of high-order nonlinear spectral profiles.

1. Introduction

In the past ten years, as a high-order nonlinear spectroscopy technique, coherent anti-Stokes Raman spectroscopy (CARS) and its surface enhancement methods [1–6] and coherent anti-Stokes hyper-Raman spectroscopy (CAHRS) [7–9] have gained important applications in kinetic processes, gene expression profile screening, high-resolution spectroscopy, nonlinear high-resolution imaging technology, and so on. However, the abovementioned research only carried out qualitative analysis of spectral signals and lacked quantitative analysis of spectral signals. This limits its application to some extent. As a high-order nonlinear coherent optical process, the spectral signals of CARS and CAHRS are contributed by the third and fourth-order microscopic polarizability tensor elements of molecular groups [10]. For n-order nonlinear coherence spectroscopy, the number of molecular microscopic polarizability tensor elements is 3^{n+1}. For example, CARS involves 81 molecular microscopic polarizability tensor elements. These large numbers of molecular microscopic polarizability tensor elements will lead to greater difficulties in the quantitative analysis of high-order nonlinear coherent optical processes [10]. In addition, in view of the nonlinearity of CARS and CAHRS, the complexity of such approaches results increased. In order to facilitate the analysis of the results, the most commonly used experimental configuration is the vertical incidence type [2]. However, with the in-depth study of the theory of high-

order nonlinear optical processes and the development of high-order nonlinear optical technologies, experimental techniques and experimental methods will gradually be improved. In the case of noncollinear experimental configurations with non-normal incidence, the acquisition of the high-order microscopic polarizability tensor element is particularly important for the quantitative analysis of spectral signals.

Based on the second-order nonlinear optical process of the sum frequency generation vibrational spectroscopy (SFG-VS) quantitative analysis method [11–13], we propose a method to simplify the high-order microscopic polarizability tensor elements of CARS and CAHRS [10, 14]. By analyzing the symmetry of molecular groups, the number of independent nonzero high-order microscopic polarizability tensor elements are reduced. Thus, CARS microscopic polarizability tensor element $\beta_{i'j'k'l'}$ is expressed as the product of two Raman microscopic polarizability tensor elements differential $\alpha'_{i'j'}$ and $\alpha'_{k'l'}$. The microscopic polarizability tensor element of CAHRS $\beta_{i'j'k'l'm'}$ is expressed as the product of the hyper-Raman microscopic polarizability tensor element differential $\beta'_{i'j'k'}$ and the Raman microscopic polarizability tensor element differential $\alpha'_{l'm'}$. The ratio between $\beta_{i'j'k'l'}$ and $\beta_{i'j'k'l'm'}$ could be simplified by using the ratio between $\alpha'_{i'j'}$ and $\beta'_{i'j'k'}$. Therefore, the problem of solving the ratio of high-order microscopic polarizability tensor elements is simplified to the problem of solving the ratio of two low-order microscopic polarizability tensor elements differential. Finally, the problem comes down to how to find the ratio of Raman and hyper-Raman microscopic polarizability tensor elements differential. In the literature [11, 14], the 2-order, 3-order, and 4-order microscopic polarizability tensor elements expressed by the hyper-Raman microscopic polarizability tensor element differential $\beta'_{i'j'k'}$, the Raman microscopic polarizability tensor element differential $\alpha'_{i'j'}$, and the dipole moment tensor element differentials $\mu'_{i'}$ are as follows:

$$\beta_{i'j'k'} = -\frac{1}{2\omega_q \varepsilon_0}\alpha'_{i'j'} \cdot \mu'_{k'}, \tag{1}$$

$$\beta_{i'j'k'l'} = -\frac{1}{2\omega_q \varepsilon_0}\alpha'_{i'j'} \cdot \alpha_{k'l'}, \tag{2}$$

$$\beta_{i'j'k'l'm'} = -\frac{1}{2\omega_q \varepsilon_0}\beta'_{i'j'k'} \cdot \alpha_{l'm'}. \tag{3}$$

When we get the ratio between $\mu'_{i'}$, $\alpha'_{i'j'}$, and $\beta'_{i'j'k'}$, we can obtain the proportional relationship between the microscopic polarizability tensor elements of CARS and CAHRS of CO_2 through the expressions (3)–(5).

Bond additivity model (BAM) is usually used to solve the ratio of Raman microscopic polarizability tensor elements differential in literature [11, 15, 16]. Notably, when Wang group [17] discussed the SFG-VS signal at the air/methanol interface, it was found that the ratio between the differential $\alpha'_{i'j'}$ of the Raman microscopic polarizability tensor derived from the traditional BAM was brought into the SFG-VS quantitative analysis method, and the results were inconsistent with the experimental measurement. Therefore, the results of BAM are corrected by the method of experimental correction, so that the results are in good agreement with the measured interface sum-frequency vibration spectra. In this paper, by using the BAM and its experimental modification, a simplified scheme is proposed to calculate the hyper-Raman microscopic polarizability tensor differential $\beta'i'j'k'$ of the carbon dioxide (CO_2) molecule. This approach is quite general, and it can be extended to other nonlinear coherent Raman spectroscopic techniques to simplify the relationship between the microscopic polarizability tensor elements and quantitative analysis of the experimental signal, such as time-domain Raman spectroscopy [18, 19], stimulated Raman scattering [20, 21], and nonlinear high-resolution microscopy [5, 6]. In order to carry out this work, the anharmonic mode couplings and higher-order corrections to the molecular polarizabilities have been neglected in this paper.

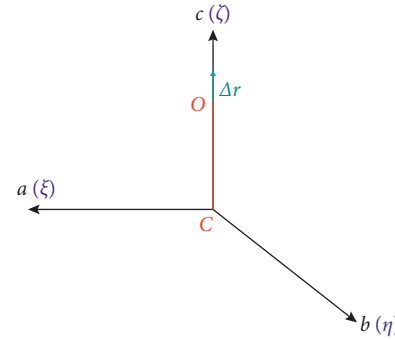

Figure 1: Molecular coordinate system of $(C)_{\infty v}$ symmetric molecular group.

2. BAM Solves $\beta'_{i'j'k'}$ of Single Bond

The BAM method is based on the assumption of the local mode of a molecular group and the assumption of the local mode of a single bond. In this model, the hyper-Raman microscopic polarizability corresponding to the stretching vibration of a single bond in the group is coupled by symmetry analysis, and the expression of the hyper-Raman microscopic polarizability tensor differential corresponding to each normal vibration mode of the molecular group is obtained. In the BAM method, the discussion of a single bond is the basis of the whole molecular group discussion. Therefore, we first discuss the $\beta'_{i'j'k'}$ of single bond CO with $C_{\infty v}$ symmetry in Figure 1.

The reduced mass G_{A1} of single bond CO and the normal coordinate Q_{A1} of symmetric vibration mode are as defined as follows [17]:

$$G_{A_1} = \frac{1}{M_C} + \frac{1}{M_O}, \tag{4}$$

$$Q_{A_1} = \frac{|\Delta \mathbf{r}|}{\sqrt{G_{A_1}}}. \tag{5}$$

M_C and M_O are the masses of carbon and oxygen atom, and $_{\Delta\mathbf{r}}$ is the vibration vector of CO along the ζ-axis in the bond coordinate system (ξ,η,ζ). It can be seen from expressions (5) that

$$|\Delta\mathbf{r}| = Q_{A_1}\sqrt{G_{A_1}}. \tag{6}$$

For CO, the molecular coordinate system (a,b,c) coincides with the bond coordinate system (ξ,η,ζ), so the three projection components of the vibration vector $_{\Delta\mathbf{r}}$ in the molecular coordinate system (a,b,c) are

$$(\Delta\mathbf{r})_a = 0, \tag{7}$$

$$(\Delta\mathbf{r})_b = 0, \tag{8}$$

$$(\Delta\mathbf{r})_c = |\Delta\mathbf{r}|. \tag{9}$$

The relationships between the hyper-Raman microscopic polarizability tensor element differentiation of CO are as follows:

$$\beta_{\zeta\xi\xi}' = \beta_{\zeta\eta\eta}' = r_1\beta_{\zeta\zeta\zeta}',\ \beta_{\xi\xi\zeta}' = \beta_{\xi\zeta\xi}' = \beta_{\eta\eta\zeta}' = \beta_{\eta\zeta\eta}' = r_2\beta_{\zeta\zeta\zeta}'. \tag{10}$$

Above $\beta'_{\xi\eta\zeta} = \partial\beta_{\xi\eta\zeta}/\partial\Delta\zeta$, $\Delta\zeta = |_{\Delta\mathbf{r}}|$ is the mode of the vibration vector $_{\Delta\mathbf{r}}$ along the ζ-axis. r_1 and r_2 are the ratios of the differential of the hyper-Raman microscopic polarizability tensor of CO. For the convenience of calculation, the $\beta_0 = \partial\beta_{\zeta\zeta\zeta}/\partial\Delta\zeta$. According to the definition of molecular group dipole moment, three components of single bond AB dipole moment in the bond coordinate system are as follows:

$$\mu_\xi = \beta_0\left(r_2E_\zeta E_\xi + r_2E_\xi E_\zeta\right)\Delta\zeta = 2\beta_0 r_2E_\xi E_\zeta\Delta\zeta, \tag{11}$$

$$\mu_\eta = \beta_0\left(r_2E_\zeta E_\eta + r_2E_\eta E_\zeta\right)\Delta\zeta = 2\beta_0 r_2E_\eta E_\zeta\Delta\zeta, \tag{12}$$

$$\mu_\zeta = \beta_0\left(r_1E_\xi E_\xi + r_1E_\eta E_\eta + E_\zeta E_\zeta\right)\Delta\zeta, \tag{13}$$

where E_ξ, E_η, and E_ζ represent the projection of the external light field in the bond coordinate system. The expressions (11)–(13) are transformed into the molecular coordinate system, and the results are as follows:

$$\mu_a = \beta_0\left(r_2E_cE_a + r_2E_aE_c\right)|\Delta\mathbf{r}| = 2\beta_0 r_2E_aE_c|\Delta\mathbf{r}|, \tag{14}$$

$$\mu_b = \beta_0\left(r_2E_cE_b + r_2E_bE_c\right)|\Delta\mathbf{r}| = 2\beta_0 r_2E_bE_c|\Delta\mathbf{r}|, \tag{15}$$

$$\mu_c = \beta_0\left(r_1E_aE_a + r_1E_bE_b + E_cE_c\right)|\Delta\mathbf{r}|. \tag{16}$$

We take the expression (6) of $|_{\Delta\mathbf{r}}|$ into expressions (14)–(16), compared with the dipole moment expression $\mu_{i'} = \sum_{j',k'=a,b,c}\beta_{i'j'k'}E_{j'}E_{k'}$ in the molecular coordinate system, and the expressions of the hyper-Raman microscopic polarizability tensor $\beta_{i'j'k'}$ are as follows:

$$\beta_{aac} = \beta_{aca} = \beta_{bbc} = \beta_{bcb} = r_2\beta_0Q_{A_1}\sqrt{G_{A_1}}, \tag{17}$$

$$\beta_{caa} = \beta_{cbb} = r_1\beta_0Q_{A_1}\sqrt{G_{A_1}}, \tag{18}$$

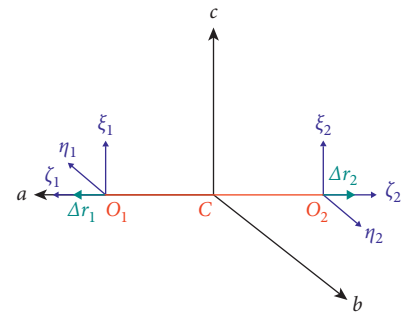

Figure 2: Molecular coordinate system of CO_2.

$$\beta_{ccc} = \beta_0Q_{A_1}\sqrt{G_{A_1}}, \tag{19}$$

take $\beta_{i'j'k'}$ derivative of Q_{A1}. The expressions of the hyper-Raman microscopic polarizability tensor differential $\beta'_{i'j'k'}$ of CO are as follows:

$$\beta'_{aac} = \beta'_{aca} = \beta'_{bbc} = \beta'_{bcb} = r_2\beta_0\sqrt{G_{A_1}}, \tag{20}$$

$$\beta'_{cca} = \beta'_{cbb} = r_1\beta_0\sqrt{G_{A_1}}, \tag{21}$$

$$\beta'_{ccc} = \beta_0\sqrt{G_{A_1}}, \tag{22}$$

from expressions (20)–(22), the ratios r_1^{HR} and r_2^{HR} of $\beta'_{i'j'k'}$ for the $C_{\infty V}$ symmetry molecular group in reference [14] can be simplified as follows:

$$r_1^{HR} = \frac{\beta_{caa}'}{\beta_{ccc}'} = r_1, \tag{23}$$

$$r_2^{HR} = \frac{\beta_{aac}'}{\beta_{ccc}'} = r_2. \tag{24}$$

3. BAM Solves $\beta'_{i'j'k'}$ of CO_2

Coupling the $\beta'_{i'j'k'}$ of two single bond CO, the expression of $\beta'_{i'j'k'}$ of CO_2 can be obtained.

For CO_2 shown in Figure 2, the normal coordinates Q_{A1} and Q_{B1} of CO_2 are defined as follows [17]:

$$Q_{A_1} = \frac{\left(|\Delta\mathbf{r}_1| + |\Delta\mathbf{r}_2|\right)}{\sqrt{2G_{A_1}}}, \tag{25}$$

$$Q_{B_1} = \frac{\left(|\Delta\mathbf{r}_1| - |\Delta\mathbf{r}_2|\right)}{\sqrt{2G_{B_1}}}, \tag{26}$$

in which, $|_{\Delta\mathbf{r}\ i}|$ is the modulus of vibration vector of CO_i, which is along the ζ_i axis in the bond coordinate system (ξ_i,η_i,ζ_i), G_{A1} and G_{B1} are the reciprocal of reduced masses, and the expression of G_{A1} and G_{B1} are as follows [17]:

$$G_{A_1} = \frac{1}{M_B}, \tag{27}$$

$$G_{B_1} = \frac{2}{M_A} + \frac{1}{M_B}. \tag{28}$$

It can be seen from expressions (25) and (26) that

$$\left|\Delta \mathbf{r}_1\right| = \frac{1}{2}\left(Q_{A_1}\sqrt{2G_{A_1}} + Q_{B_1}\sqrt{2G_{B_1}}\right), \tag{29}$$

$$\left|\Delta \mathbf{r}_2\right| = \frac{1}{2}\left(Q_{A_1}\sqrt{2G_{A_1}} - Q_{B_1}\sqrt{2G_{B_1}}\right). \tag{30}$$

From Figure 2, the projection components of the vibration vectors $_{\Delta \mathbf{r}1}$ and $_{\Delta \mathbf{r}2}$ in the molecular coordinate system are as follows:

$$(\Delta \mathbf{r}_1)_a = \left|\Delta \mathbf{r}_1\right|, (\Delta \mathbf{r}_1)_b = 0, (\Delta \mathbf{r}_1)_c = 0, \tag{31}$$

$$(\Delta \mathbf{r}_2)_a = -\left|\Delta \mathbf{r}_2\right|, (\Delta \mathbf{r}_2)_b = 0, (\Delta \mathbf{r}_2)_c = 0. \tag{32}$$

According to the definition of molecular group dipole moment, three components of CO_i ($i = 1,2$) dipole moment in the bond coordinate system are as follows:

$$\mu_{\xi_i} = \beta_0\left(r_2 E_{\zeta_i} E_{\xi_i} + r_2 E_{\xi_i} E_{\zeta_i}\right)\left|\Delta \mathbf{r}_i\right| = 2\beta_0 r_2 E_{\xi_i} E_{\zeta_i}\left|\Delta \mathbf{r}_i\right|, \tag{33}$$

$$\mu_{\eta_i} = \beta_0\left(r_2 E_{\zeta_i} E_{\eta_i} + r_2 E_{\eta_i} E_{\zeta_i}\right)\left|\Delta \mathbf{r}_i\right| = 2\beta_0 r_2 E_{\eta_i} E_{\zeta_i}\left|\Delta \mathbf{r}_i\right|, \tag{34}$$

$$\mu_{\zeta_i} = \beta_0\left(r_1 E_{\xi_i} E_{\xi_i} + r_1 E_{\eta_i} E_{\eta_i} + E_{\zeta_i} E_{\zeta_i}\right)\left|\Delta \mathbf{r}_i\right|. \tag{35}$$

The bonds CO_1 and CO_2 are identical except for orientation, so β_0, r_1, and r_2 of the two single bonds are the same. $E_{\xi i}$, $E_{\eta i}$, and $E_{\zeta i}$ represent the projection of the external light field in the bond coordinate system. From Figure 2, the expressions of $E_{\xi i}$, $E_{\eta i}$, and $E_{\zeta i}$ are as follows:

$$E_{\xi_1} = E_c, E_{\eta_1} = -E_b, E_{\zeta_1} = E_a, \tag{36}$$

$$E_{\xi_2} = E_c, E_{\eta_2} = E_b, E_{\zeta_2} = -E_a. \tag{37}$$

By projecting the dipole moments of two single bonds into the molecular coordinate system and adding them together, the results are as follows:

$$\mu_a = \mu_{\zeta_1} - \mu_{\zeta_2}, \tag{38}$$

$$\mu_b = -\mu_{\eta_1} + \mu_{\eta_2}, \tag{39}$$

$$\mu_c = \mu_{\xi_1} + \mu_{\xi_2}. \tag{40}$$

By comparing the expressions (38)–(40) with the expressions of dipole moment in the molecular coordinate system $\mu_{i'} = \sum_{j',k'=a,b,c}\beta_{i'j'k'}E_{j'}E_{k'}$, the expressions of $\beta_{i'j'k'}$ are as follows:

$$\beta_{ccc} = \beta_{caa} = \beta_{cbb} = \beta_{aac} = \beta_{aca} = \beta_{bbc} = \beta_{bcb} = 0, \tag{41}$$

$$\beta_{aaa} = \beta_0\left(\left|\Delta \mathbf{r}_1\right| - \left|\Delta \mathbf{r}_2\right|\right), \tag{42}$$

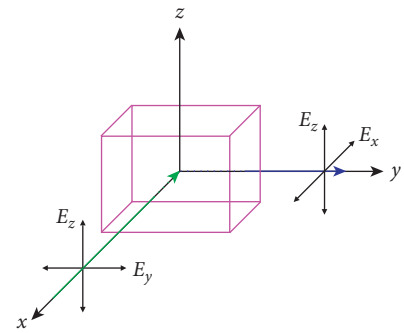

Figure 3: The experimental optical path for measuring the hyper-Raman depolarization rate.

$$\beta_{acc} = \beta_{abb} = r_1\beta_0\left(\left|\Delta \mathbf{r}_1\right| - \left|\Delta \mathbf{r}_2\right|\right), \tag{43}$$

$$\beta_{cca} = \beta_{cac} = \beta_{bba} = \beta_{bab} = r_2\beta_0\left(\left|\Delta \mathbf{r}_1\right| - \left|\Delta \mathbf{r}_2\right|\right). \tag{44}$$

From expression (26), we could derive that

$$\left|\Delta \mathbf{r}_1\right| - \left|\Delta \mathbf{r}_2\right| = Q_{B_1}\sqrt{2G_{B_1}}. \tag{45}$$

Substituting expression (45) into expressions (41)–(44), we obtain the $\beta_{i'j'k'}$ derivative of Q_{B1}, the expressions of $\beta'_{i'j'k'}$ for the antisymmetric vibration mode are as follows:

$$\beta'^{AS}_{ccc} = \beta'^{AS}_{caa} = \beta'^{AS}_{cbb} = \beta'^{AS}_{aac} = \beta'^{AS}_{aca} = \beta'^{AS}_{bbc} = \beta'^{AS}_{bcb} = 0, \tag{46}$$

$$\beta'^{AS}_{aaa} = \beta_0\sqrt{2G_{B_1}}, \tag{47}$$

$$\beta'^{AS}_{acc} = \beta'^{AS}_{abb} = r_1\beta_0\sqrt{2G_{B_1}}, \tag{48}$$

$$\beta'^{AS}_{cca} = \beta'^{AS}_{cac} = \beta'^{AS}_{bba} = \beta'^{AS}_{bab} = r_2\beta_0\sqrt{2G_{B_1}}. \tag{49}$$

From the expressions (46)–(49), the relationship of $\beta'_{i'j'k'}$ for the antisymmetric vibration mode are as follows:

$$R^{HR}_{AS,a_1} = \frac{\beta'^{AS}_{acc}}{\beta'^{AS}_{aaa}} = R^{HR}_{AS,b_1} = \frac{\beta'^{AS}_{abb}}{\beta'^{AS}_{aaa}} = r_1, \tag{50}$$

$$R^{HR}_{AS,a_2} = \frac{\beta'^{AS}_{cca}}{\beta'^{AS}_{aaa}} = R^{HR}_{AS,b_2} = \frac{\beta'^{AS}_{bba}}{\beta'^{AS}_{aaa}} = r_2. \tag{51}$$

From the expressions (50)–(51), the ratios R^{HR}_{AS,a_1}, R^{HR}_{AS,b_1}, R^{HR}_{AS,a_2}, and R^{HR}_{AS,b_2}, are only related to r_1 and r_2 of single bond CO. And r_1 and r_2 can be obtained by measuring the hyper-Raman depolarization rate [17].

4. Experimental Correction of r_1 and r_2

The ratios of r_1 and r_2 can be obtained by experimentally measuring the hyper-Raman depolarization rate [22]. The experimental optical path for measuring the hyper-Raman depolarization rate is shown in Figure 3. (x,y,z) represents the laboratory coordinate system. The direction of the

incident light is parallel (H) to or perpendicular (V) to the horizontal plane (*xy* plane). The outgoing light is detected in a direction at a 90° angle to the incident light, and the detected polarization direction is the vertical (V) direction. By selecting the polarization of the incident and outgoing light, the signals I_{HV} and I_{VV} of the two polarization combinations can be obtained. The expression of the hyper-Raman depolarization rate of a certain vibrational mode of the studied molecule is shown in expression (52), and $\langle \beta'^{2}_{IJK} \rangle$ $(I,J,K = x,y,z)$ is shown in expression (53) [19].

$$\rho = \frac{I_{HV}}{I_{VV}} = \frac{\langle \beta'^{2}_{zyy} \rangle}{\langle \beta'^{2}_{zzz} \rangle}, \tag{52}$$

$$\langle \beta'^{IJK2} \rangle = \sum_{i,j,k,i',j',k'} \beta'_{ijk}\beta_{i'j'k'} \int_0^{2\pi}\int_0^{2\pi}\int_0^{\pi} R_{Ii}R_{Jj}R_{Kk}R_{Ii'}R_{Jj'}R_{Kk'} \sin\theta \, d\theta \, d\psi \, d\phi \Big/ \int_0^{2\pi}\int_0^{2\pi}\int_0^{\pi} \sin\theta \, d\theta \, d\psi \, d\phi. \tag{53}$$

In which R_{Ii} is the matrix element of the Euler transformation from the molecular coordinate system to the laboratory coordinate system, β'_{ijk} is the hyper-Raman microscopic polarizability tensor differentials. The expressions (46)–(49) are introduced into expression (53) to obtain the relationship between the hyper-Raman depolarization rate and the r_1, r_2, and τ. If for a certain molecular group, can be measured to the symmetric vibration mode of the hyper-Raman depolarization rate ρ_{SS} and antisymmetric vibration mode of the hyper-Raman depolarization rate ρ_{AS}, we could be using the values of ρ_{SS} and ρ_{AS} to determine the value of r_1 and r_2.

For example, for the CO_2 which is C_{2v} symmetric type, the bond angle $\tau = 180°$, $M_C = 12$, and $M_O = 16$. The ρ_{SS} and ρ_{AS} are shown in the expressions (54) and (55), respectively.

$$\rho_{SS} = \frac{I_{HV-SS}}{I_{VV-SS}} = \frac{24 + 8r_1 - 96r_2 - 16r_1r_2 + 108r_1^2 + 96r_2^2}{39 + 6r_1 + 12r_2 + 100r_1r_2 + 25r_1^2 + 100r_2^2}, \tag{54}$$

$$\rho_{AS} = \frac{I_{HV-AS}}{I_{VV-AS}} = \frac{8 + 40r_1 - 32r_2 - 80r_1r_2 + 92r_1^2 + 32r_2^2}{55 + 62r_1 + 116r_2 + 100r_1r_2 + 23r_1^2 + 108r_2^2}. \tag{55}$$

The value of r_1 and r_2 can be solved by taking the experimental measured ρ_{HR}^{SS} and ρ_{HR}^{AS} into expressions (54) and (55).

Using the experimentally modified BAM method, we can get the ratio of the hyper-Raman microscopic polarizability tensor element differentials that is consistent with the experimental results. Combining the ratio between the Raman microscopic polarizability tensor differentials, and bringing the above relation into the expressions (50) and (51), we can greatly simplify the relationship between CARS and CAHRS microscopic polarizability tensors.

Through the presented analysis, we obtained the ratios between the hyper-Raman microscopic polarizability tensor element differentials $\beta'_{i'j'k'}$. Combining the ratios between Raman microscopic polarizability tensor element differentials $\alpha'_{i'j'}$ in the literature, we obtain the proportional relationship between the microscopic polarizability tensor element of CARS and CAHRS.

5. Conclusions

In this paper, a simplified method of microscopic polarizability tensor differential of hyper-Raman spectroscopy based on BAM is investigated. In the first, we use the differentiation of Raman microscopic polarizability tensor $\alpha'_{i'j'}$ and the hyper-Raman microscopic polarizability tensor $\beta'_{i'j'k'}$ to mean the CARS and CAHRS microscopic hyperpolarizability tensor elements, so the high-order spectra can be simplified to the analysis of low-order spectra. Then, taking the CO_2 molecule as an example, we use the bond additivity model method to analyze the normal vibration mode of the single bond stretching vibration to obtain the hyper-Raman microscopic polarizability tensor element differential $\beta'_{i'j'k'}$ of the single bond CO. On that basis, by analyzing the symmetry of the CO_2 molecule, the $\beta'_{i'j'k'}$ of the two single bonds are vector-coupled to obtain the expressions of the hyper-Raman microscopic polarizability tensor element differential $\beta'_{i'j'k'}$ of the two normal vibration modes of the CO_2 molecule. Finally, combining the ratios between Raman microscopic polarizability tensor element differentials $\alpha'_{i'j}$, we derived the relationship between the microscopic polarizability tensor element of CARS and CAHRS. The above analysis provides a theoretical basis for the quantitative analysis of high-order nonlinear spectral signals in symmetric molecular systems with 2 or 3 atoms.

This approach is quite general, and it can be extended to other nonlinear coherent Raman spectroscopic techniques to simplify the relationship between the microscopic polarizability tensor elements and quantitative analysis of the experimental signal, such as time-domain Raman spectroscopy, stimulated Raman scattering, and nonlinear high-resolution microscopy.

Data Availability

No data were used to support this study.

Conflicts of Interest

The authors declare that they have no conflicts of interest.

References

[1] W. M. Pazin, L. N. Furini, V. Solovyeva et al., "Vibrational spectroscopic characterization and coherent anti-Stokes Raman spectroscopy (CARS) imaging of artepillin C," *Applied Spectroscopy*, vol. 74, no. 7, pp. 751–757, 2020.

[2] T. Hollon, S. Lewis, C. W. Freudiger, X Sunney Xie, and D. A Orringer, "Improving the accuracy of brain tumor surgery via Raman-based technology," *Neurosurgical Focus*, vol. 40, no. 3, p. E9, 2016.

[3] G. Liu, F. A. Narducci, and S. A. Malinovskaya, "Limits to remote molecular detection via coherent anti-Stokes Raman spectroscopy using a maximal coherence control technique," *Journal of Modern Optics*, vol. 67, no. 1, pp. 21–25, 2020.

[4] Y. J. Peng, S. Sun, and Y. F. Song, "Coherent anti-Stokes Raman scattering spectrum of vibrational properties of liquid nitromethane molecules," *Acta Physica Sinica*, vol. 67, no. 2, Article ID 024208, 2018.

[5] D. Polli, V. Kumar, C. M. Valensise, M. Marangoni, and G. Cerullo, "Broadband coherent Raman scattering microscopy," *Laser & Photonics Reviews*, vol. 12, no. 9, Article ID 1800020, 2018.

[6] R. C. Prince, R. R. Frontiera, and E. O. Potma, "Stimulated Raman scattering: from bulk to nano," *Chemical Reviews*, vol. 117, no. 7, pp. 5070–5094, 2017.

[7] G. Fumero, G. Batignani, K. E. Dorfman, S. Mukamel, and T. Scopigno, "On the resolution limit of femtosecond stimulated Raman spectroscopy: modelling fifth-order signals with overlapping pulses," *ChemPhysChem*, vol. 16, no. 16, pp. 3438–3443, 2015.

[8] G. Fumero, C. Schnedermann, and G. Batignani, "Two-dimensional impulsively stimulated resonant Raman spectroscopy of molecular excited states," *Physical Review X*, vol. 10, no. 1, Article ID 011051, 2020.

[9] Z. Zhang, K. Bennett, V. Chernyak, and S. Mukamel, "Utilizing microcavities to suppress third-order cascades in fifth-order Raman spectra," *The Journal of Physical Chemistry Letters*, vol. 8, no. 14, pp. 3387–3391, 2017.

[10] Y. Wang, Z.-f. Cui, and H.-f. Wang, "Experimental observables and macroscopic susceptibility/microscopic polarizability tensors for third and fourth-order nonlinear spectroscopy of ordered molecular system," *Chinese Journal of Chemical Physics*, vol. 20, no. 4, pp. 449–460, 2007.

[11] H.-F. Wang, W. Gan, R. Lu, Y. Rao, and B.-H. Wu, "Quantitative spectral and orientational analysis in surface sum frequency generation vibrational spectroscopy (SFG-VS)," *International Reviews in Physical Chemistry*, vol. 24, no. 2, pp. 191–256, 2005.

[12] H.-F. Wang, "Sum frequency generation vibrational spectroscopy (SFG-VS) for complex molecular surfaces and interfaces: spectral lineshape measurement and analysis plus some controversial issues," *Progress in Surface Science*, vol. 91, no. 4, pp. 155–182, 2016.

[13] H.-F. Wang, L. Velarde, W. Gan, and L. Fu, "Quantitative sum-frequency generation vibrational spectroscopy of molecular surfaces and interfaces: lineshape, polarization, and orientation," *Annual Review of Physical Chemistry*, vol. 66, no. 1, pp. 189–216, 2015.

[14] Y. Wang, Z. Zhang, and Y. Guo, "A simplified method of microscopic hyperpolarizability of coherent anti-Stokes Raman spectroscopy and coherent anti-Stokes hyper-Raman spectroscopy-$C_{\infty v}$ symmetry," *Spectroscopy and Spectral Analysis*, vol. 39, no. 2, pp. 465–470, 2019.

[15] X. Wei, S.-C. Hong, X. Zhuang, T. Goto, and Y. R. Shen, "Nonlinear optical studies of liquid crystal alignment on a rubbed polyvinyl alcohol surface," *Physical Review*, vol. 62, no. 4, pp. 5160–5172, 2000.

[16] D. Zhang, J. Gutow, and K. B. Eisenthal, "Vibrational spectra, orientations, and phase transitions in long-chain amphiphiles at the air/water interface: probing the head and tail groups by sum frequency generation," *Journal of Physical Chemistry*, vol. 98, no. 51, pp. 13729–13734, 1994.

[17] H. Wu, W. K. Zhang, W. Gan, W. K. Zhang, W. Gan, and Z. F. Cui, "Wang HF "an empirical approach to the bond additivity model in quantitative interpretation of sum frequency generation vibrational spectra"," *The Journal of Chemical Physics*, vol. 125, no. 13, Article ID 133203, 2006.

[18] G. Batignani, C. Ferrante, G. Fumero, and T. Scopigno, "Broadband impulsive stimulated Raman scattering based on a chirped detection," *The Journal of Physical Chemistry Letters*, vol. 10, no. 24, pp. 7789–7796, 2019.

[19] M. Liebel and P. Kukura, "Broad-band impulsive vibrational spectroscopy of excited electronic states in the time domain," *The Journal of Physical Chemistry Letters*, vol. 4, no. 8, pp. 1358–1364, 2013.

[20] P. Kukura, D. W. McCamant, and R. A. Mathies, "Femtosecond stimulated Raman spectroscopy," *Annual Review of Physical Chemistry*, vol. 58, no. 1, pp. 461–488, 2007.

[21] G. Batignani, C. Ferrante, and T. Scopigno, "Accessing excited state molecular vibrations by femtosecond stimulated Raman spectroscopy," *The Journal of Physical Chemistry Letters*, vol. 11, no. 18, pp. 7805–7813, 2020.

[22] O. Quinet, B. Champagne, and V. Rodriguez, "Experimental and theoretical investigation of the Raman and hyper-Raman spectra of acetonitrile and its derivatives," *The Journal of Chemical Physics*, vol. 124, no. 24, Article ID 244312, 2006.